1 **Secondary Organic Aerosol Formation from Nitrate Radical Oxidation of Styrene: Aerosol**
2 **Yields, Chemical Composition, and Hydrolysis of Organic Nitrates**

3

4 Yuchen Wang[1,2], Xiang Zhang[1], Yuanlong Huang[3], Yutong Liang[2,6], Nga L. Ng*[,2,4,5]

5

6 [1] College of Environmental Science and Engineering, Hunan University, Changsha, Hunan, 410082, China
7 [2] School of Chemical and Bimolecular Engineering, Georgia Institute of Technology, Atlanta, Georgia
8 30332, USA
9 [3] Ningbo Institute of Digital Twin, Eastern Institute of Technology, Ningbo, 315200, China
10 [4] School of Civil and Environmental Engineering, Georgia Institute of Technology, Atlanta, Georgia 30332,
11 USA
12 [5] School of Earth and Atmospheric Sciences, Georgia Institute of Technology, Atlanta, Georgia 30332,
13 USA
14 [6] Thrust of Sustainable Energy and Environment, The Hong Kong University of Science and Technology
15 (Guangzhou), Guangdong, 511453, China
16 *Corresponding Author: Nga L. Ng (ng@chbe.gatech.edu)

17

18 **Abstract**

19 Styrene is emitted from anthropogenic sources and biomass burning and is highly reactive towards
20 atmospheric oxidants. While it has the highest nitrate radical (NO_3) reactivity among aromatic
21 hydrocarbons, the NO_3 oxidation of styrene and formation mechanisms of secondary organic aerosols (SOA)
22 have not been investigated. In this study, we conduct chamber experiments with styrene concentrations
23 ranging from 9.5-155.2 ppb. The resulting SOA yields range from 14.0-22.1% with the aerosol mass
24 loadings of 5.9-147.6 µg/m³ after wall loss corrections. The chemical composition of SOA is characterized
25 by online measurements, revealing that dimeric organic nitrates (ONs) constitute 90.9% of the total signal
26 of particle-phase products. $C_{16}H_{16}N_2O_8$ and $C_8H_9NO_4$ are identified as the major particle-phase products,
27 which constitute 88.3% and 4.1% of the measured signal, respectively. We propose formation mechanisms
28 for the ON products, including the common RO_2+RO_2/HO_2 pathway and other radical chain termination
29 reactions such as RO+R and R+R. We also investigate the hydrolysis of particulate ONs. The hydrolysis
30 lifetime for ONs is determined to be less than 30 minutes. This short hydrolysis lifetime can be attributed
31 to the stabilization of the carbocation by delocalized π orbitals of the benzene-related skeleton of aromatic
32 ONs. This work provides the first fundamental laboratory data to evaluate SOA production from
33 styrene+NO_3 chemistry. Additionally, the formation mechanisms of aromatic ONs are reported for the first
34 time, highlighting that compounds previously identified as nitroaromatics in ambient field campaigns could
35 also be attributed to aromatic ONs.

36

37 **Keywords:** Styrene, secondary organic aerosols, aerosol yields, organic nitrate, organonitrate, vapor wall
38 loss, biomass burning

1. Introduction

39

40   Aromatic hydrocarbons are a class of unsaturated chemical compounds characterized by the presence

41 of delocalized π orbitals. They play a crucial role in the atmosphere, contributing up to 60% of volatile

42 organic compounds (VOCs) in urban environments (Calvert et al., 2002; Cabrera-Perez et al., 2016).

43 Styrene is particularly unique within aromatic hydrocarbons as it possesses both an unsaturated double bond

44 and a benzene ring and has the combined properties of alkenes and aromatic compounds. Although styrene

45 is not the most abundant aromatic hydrocarbon, with concentrations ranging from 0.06 to 45 ppb in the

46 atmosphere (Cho et al., 2014; Tuazon et al., 1993), it has the highest reaction rate constants for reactions

47 with hydroxyl radicals (OH), nitrate radicals (NO_3), ozone (O_3), and chlorine radicals because of the

48 unsaturated double bond (Tuazon et al., 1993; Tajuelo et al., 2019a, b; Atkinson and Aschmann, 1988; Le

49 Person et al., 2008; Cho et al., 2014). In addition, styrene is the second most efficient aromatic hydrocarbon

50 in forming secondary organic aerosols (SOA) during daytime chemistry, surpassed only by toluene (Sun et

51 al., 2016). SOA yields from OH-initiated photooxidation of styrene can reach as high as around 35% for an

52 aerosol mass loading of 430 μg/m^3 (Schueneman et al., 2024). A theoretical study suggests that OH-initiated

53 photooxidation of styrene could be a substantial contributor to SOA formation in urban environments (Wang

54 et al., 2015).

55   To the best of our knowledge, no study has specifically investigated SOA formation from styrene+NO_3

56 oxidation. Although styrene emissions from various anthropogenic sources such as industrial activities,

57 motor vehicle operations, combustion processes, building materials, or consumer products (Zhang et al.,

58 2017; Knighton et al., 2012; Helal and Elshafy, 2012; Okada et al., 2012), are predominantly active during

59 the daytime, high levels of styrene have also been observed at night in urban environments. The nighttime

60 presence of styrene is likely influenced by the boundary layer accumulation effect (Wu et al., 2020; Lu et

61 al., 2023a), which enhances the conditions for styrene+NO_3 oxidation. Additionally, biomass burning,

62 particularly wildfires, contributes to emission of styrene in rural and forest regions (Koss et al., 2018). The

63 NO_3 oxidation of styrene can occur under conditions such as nighttime chemistry or optically dense plumes

64 during biomass burning events (Decker et al., 2021). Given that styrene exhibits the highest NO_3 reactivity

65 among aromatic hydrocarbons (Yang et al., 2020), the styrene+NO_3 oxidation can play a major role in the

66 consumption of styrene and formation of SOA.

67   The NO_3 oxidation of VOCs is also expected to generate a substantial quantity of organic nitrates

68 (ONs), primarily through the direct incorporation of the NO_3 with the double bond during reactions (Ng et

69 al., 2017; Orel et al., 1978). ONs have been shown to influence NO_x recycling, O_3 production, and the

70 formation of SOA in the atmosphere (Ng et al., 2017). Ambient field measurements consistently

71 demonstrate the widespread presence of ONs derived from aromatics in submicron organic aerosols at

72 various locations globally (Lu et al., 2023b; Lin et al., 2021; Jiang et al., 2023; Yang et al., 2019). For

73   example, in Shanghai, around 16% of the oxygenated organic molecules containing two nitrogen atoms

74   originate from aromatic compounds (Lu et al., 2023b). In Beijing, the concentration of phenethyl nitrate is

75   found to be 3.23 ng m^{-3} (Yang et al., 2019). All these suggest that the oxidation of styrene by NO$_3$ could be

76   an important pathway for generating aromatic ONs.

77   Hydrolysis of particulate ONs is an important sink of NO$_x$, especially when the ONs have short

78   hydrolysis lifetimes (Pye et al., 2015; Fisher et al., 2016; Zare et al., 2019; Vasquez et al., 2021; Takeuchi

79   and Ng, 2019). To our knowledge, there is no study on hydrolysis of ONs formed from oxidation of aromatic

80   compounds. More studies focus on biogenic ONs. For instance, results from hydrolysis of biogenic ONs in

81   bulk solutions indicate that the number of alkyl substitutions, the types of functional groups, and the

82   structures of carbon skeletons are three important factors controlling hydrolysis rates (Darer et al., 2011;

83   Hu et al., 2011; Jacobs et al., 2014; Rindelaub et al., 2016; Wang et al., 2021b). A common feature identified

84   in the mechanisms is the formation of stable carbocations, which facilitates the rapid hydrolysis of ONs.

85   Previous research indicates that the benzene-related skeleton, featuring three delocalized π orbitals,

86   enhances the hyper-conjugation effect and stabilizes the carbocation (Wang et al., 2021b). Consequently,

87   ONs produced from styrene+NO$_3$ oxidation, which include such benzene-related skeletons, are likely to

88   have short hydrolysis lifetimes. However, this hypothesis has not been evaluated before, because of the lack

89   of hydrolysis studies of aromatic ONs.

90   In this study, we aim to investigate SOA formation and chemical composition from styrene+NO$_3$

91   oxidation. We conduct a series of chamber experiments in the dark under both dry and humid conditions.

92   SOA yields are determined across a wide range of initial styrene concentrations under dry conditions. The

93   chemical composition of SOA is characterized by online mass spectrometry and the SOA formation

94   mechanism is proposed based on these measurements. Additionally, we investigate hydrolysis of particulate

95   ONs. These results can be used to estimate SOA formation and transformation from NO$_3$ oxidation of

96   styrene from anthropogenic emissions and biomass burning in ambient environments.

97   ## 2. Experimental Section

98   ### 2.1. Environmental chamber experiments

99   The experimental conditions are summarized in Table 1. All experiments are performed in the Georgia

100   Tech Environmental Chamber (GTEC) Facility, which consists of two 12 m^3 Teflon chambers (Boyd et al.,

101   2015). Experiments are conducted at 295 ± 3 K and ambient pressure. Most experiments are conducted

102   under dry conditions (RH < 3%, Exp. 1-10), with the exception of two experiments (Exp. 11 and 12), which

103   are conducted under humid conditions (approximately 50% and 70%, respectively). These humid

104   experiments allow for the investigation of the hydrolysis processes of SOA.

105   A typical experiment begins with the injection of seed particles into the chamber by atomizing a dilute

106   ammonium sulfate solution (AS; 0.015 M). Subsequently, styrene (99 %, Sigma-Aldrich) is injected into

107 the chamber using a glass bulb, where the evaporation of styrene is facilitated by the flow of zero air at a

108 rate of 5 L min^{-1} through the bulb. The initial particle number and volume concentration are 2.9×10^4

109 particles cm^{-3} and 3.2×10^{10} nm^3 cm^{-3}, respectively. The initial concentration of styrene ranges from 9.5-

110 155.2 ppb. It is noted that Exp. 9 and 10 do not involve seed particle injection and are conducted specifically

111 to determine the density of styrene+NO$_3$ SOA.

112   N$_2$O$_5$ is generated by the reaction of NO$_2$ (Matheson, 500 ppm) and O$_3$ (generated by passing purified

113 air through a UV light (Jelight 610), ~125 ppm) in a flow tube (0.8 L min^{-1} flow rate, 115 s residence time)

114 and injected into the chamber as NO$_3$ precursor. The injection time ranges from 5 to 75 minutes, depending

115 on the initiation concentration of styrene. The typical styrene to N$_2$O$_5$ ratio is approximately 1:2. To ensure

116 that styrene is predominantly oxidized by NO$_3$, the concentrations of O$_3$ and the flow rates of both NO$_2$ and

117 O$_3$ are adjusted (based on results from a simple kinetic box model) to optimize N$_2$O$_5$ production while

118 minimizing O$_3$ concentration. Upon entering the chamber, N$_2$O$_5$ thermally decomposes, generating NO$_2$

119 and NO$_3$, establishing an equilibrium that marks the onset of NO$_3$ oxidation (Boyd et al., 2015; Takeuchi

120 and Ng, 2019).

121 **2.2. Gas- and particle-phase measurements**

122   The concentrations of O$_3$ and NO$_x$ are monitored with an ultraviolet absorption O$_3$ monitor (Teledyne

123 T400) and a NO$_x$ monitor (Thermo Fisher Scientific 42C) (Teledyne 200EU), respectively. A gas

124 chromatograph with flame ionization detector (GC-FID, Agilent) is used to track the decay of styrene.

125 Aerosol volume and size distributions of particles smaller than 1 μm in electrical mobility diameter are

126 measured by a scanning mobility particle sizer (SMPS) under the low-flow mode (sheath flow of 2 L min^{-1}

127). The SMPS is consisted with a differential mobility analyzer (TSI 3080) and a condensation particle

128 counter (TSI 3775).

129   A high-resolution time-of-flight aerosol mass spectrometer (HR-ToF-AMS; Aerodyne Research Inc.)

130 is used to quantitatively measure the bulk particle-phase chemical composition including organics, nitrate,

131 sulfate, ammonium, and chloride. The working principle and operation of the HR-ToF-AMS are described

132 in detail elsewhere (DeCarlo et al., 2006). Elemental analysis of the data is conducted to determine the

133 elemental composition of the bulk aerosols (Canagaratna et al., 2015). The data are analyzed using PIKA

134 v1.16I in Igor Pro 6.38B.

135   The speciated oxidized gas- and particle-phase products are measured using a high-resolution time-of-

136 flight chemical-ionization mass spectrometer coupled with the filter inlet for gases and aerosols (FIGAERO-

137 CIMS; Aerodyne Research Inc.) with iodide (I$^-$) as the reagent ion. Details on the operation of the instrument

138 has been described in previous literature (Boyd et al., 2017; Takeuchi and Ng, 2019; Nah et al., 2016b;

139 Chen et al., 2020; Lopez-Hilfiker et al., 2014). Briefly, reagent ions are generated from a cylinder containing

140 a mixture of CH$_3$I and dry N$_2$ (Airgas) and through polonium-210 source (NRD; model P-2021). The

141 instrument measures gaseous compounds by sampling air from the chamber at 1.7 L min^{-1}. At the same

142 time, particles in the chamber are collected onto a polytetrafluoroethylene filter with the sampling rate from

143 1 to 5 L min^{-1} depending on the aerosol mass concentrations. A gradually heated nitrogen gas flows over

144 the filter, evaporating oxidized organic species and transporting them into the CIMS for detection. The data

145 are analyzed using Tofware v2.5.11. All the compounds presented in this study are I^{-} adducts.

146 **2.3. Volatility Calibration**

147 In the FIGAERO-CIMS, during the thermal desorption stage, the temperature at which the maximum

148 (T_{max}) desorption signal for a particle-phase compound is observed corresponds to effective saturation mass

149 concentration (C*) (Lopez-Hilfiker et al., 2014; Thornton et al., 2020; Stark et al., 2017; Ylisirniö et al.,

150 2021). The experimental procedures for volatility calibration have been described in detail in our previous

151 study (Takeuchi et al., 2022). Briefly, the relationship between T_{max} and C* in FIGAERO-CIMS is

152 established by depositing a mixture of standards with known C* onto the filter. These standards are then

153 subjected to thermal desorption using the same thermal program applied in the chamber experiments. The

154 standards used in this study include glycolic acid ($C_2H_4O_3$), oxalic acid ($C_2H_4O_2$), malonic acid ($C_3H_3O_4$),

155 succinic acid ($C_4H_6O_4$), meso-erythritol ($C_4H_{10}O_4$), levoglucosan ($C_6H_{10}O_5$), suberic acid ($C_8H_{14}O_4$), azelaic

156 acid ($C_9H_{16}O_4$), sebacic acid ($C_{10}H_{18}O_4$), dodecanedioic acid ($C_{12}H_{22}O_4$), palmitic acid ($C_{16}H_{32}O_2$), stearic

157 acid ($C_{18}H_{36}O_2$), and behenic acid ($C_{22}H_{44}O_2$). The relationship between C* (in µg m^{-3}) at 25 °C and T_{max}

158 (in °C) obtained in this study is $\log_{10} [C^*_{25°C}] = -0.085T_{max} + 5.12$ (Figure S1) and is consistent with the

159 calibrations in Takeuchi et al. (2022).

160 **3. Results**

161 **3.1. SOA formation from NO$_3$ radical oxidation of styrene**

162 A series of chamber experiments with different initial styrene concentrations is performed to

163 investigate SOA formation from NO$_3$ oxidation of styrene (Table 1). In these experiments, the ratio of

164 styrene to N$_2$O$_5$ is maintained at 1:2 to optimize the reaction conditions, facilitating a complete consumption

165 of styrene and allowing for the analysis of the resulting products. Figure S2 presents the time series of the

166 formation of SOA during a typical experiment (Exp. 7). In all experiments, styrene is fully reacted within

167 60 minutes, and the peak aerosol concentration is typically observed within the same time range (Figure

168 S2).

169 All SOA data are corrected for particle wall loss by applying size-dependent coefficients determined

170 from wall loss experiments (Nah et al., 2017). The nucleation experiments are conducted to determine SOA

171 density. By comparing SMPS volume distribution and HR-ToF-AMS mass distribution (Bahreini et al.,

172 2005; Alfarra et al., 2006; Ng et al., 2008), the SOA density is determined to be 1.35 g/cm^3. Figure 1 shows

173 the SOA yields (Y, 4.5%–16.1% for Exp. 1-8, over a wide range of aerosol mass loadings (ΔM$_O$), 1.9–107.4

174 µg/m^3). For all experiments, peak aerosol mass concentration is obtained from the SMPS aerosol volume

175 concentration (averaged over 30 minutes at peak aerosol loading) and the calculated aerosol density. SOA

176 yields are parametrized as a function of organic mass produced using the a semi-empirical model (Odum et

177 al., 1996, 1997) based on gas-to-particle partitioning of two semi-volatile products (Eq.1). The fitting molar

178 yields (α_1 and α_2) are 0.1 and 0.09, and the fitted partitioning coefficients (K_1 and K_2) are 0.4 and 0.02 (R^2

179 = 0.997).

180 $$Y = \Delta M_O \left[\frac{\alpha_1 K_1}{1+K_1 M_O} + \frac{\alpha_2 K_2}{1+K_2 M_O} \right] \qquad \text{Eq. 1}$$

181 3.2. Chemical composition of SOA

182 A typical HR-ToF-AMS aerosol mass spectrum is shown in Figure 2 along with the National Institute

183 of Standards and Technology (NIST) mass spectra of possible styrene+NO_3 oxidation products. There are

184 a few notable ions in the aerosol mass spectrum. The signals at m/z 39 ($C_3H_3^+$), 50 ($C_4H_2^+$), 51 ($C_4H_3^+$), 52

185 ($C_4H_4^+$), 77 ($C_6H_5^+$), 78 ($C_6H_6^+$), 91 ($C_7H_7^+$), 105 ($C_7H_5O^+$), and 106 ($C_7H_6O^+$) are aromatic compound

186 signatures with benzene ring (McLafferty and Turecek, 1993). The signals at m/z 91 ($C_7H_7^+$), 105 ($C_7H_5O^+$),

187 and 106 ($C_7H_6O^+$), while not particularly significant in the mass spectra of other aromatic SOA systems (Yu

188 et al., 2014, 2016; Zhang et al., 2023; Liu et al., 2022; Chen et al., 2021), are relatively high for styrene+NO_3

189 oxidation system. However, m/z 91 ($C_7H_7^+$) is a signature ion for SOA formed from NO_3 oxidation of β-

190 pinene (Boyd et al., 2015) and photooxidation of β-caryophyllene (Tasoglou and Pandis, 2015). m/z 91

191 ($C_7H_7^+$) has also been detected as one of the major fragments of synthetic monoterpene ON standards

192 measured by HR-ToF-AMS (Takeuchi et al., 2024). Therefore, only m/z 105 ($C_7H_5O^+$) and 106 ($C_7H_6O^+$)

193 can potentially serve as useful indicators for SOA formed from styrene oxidation in ambient aerosol mass

194 spectra. Note that the HR-ToF-AMS spectrum of styrene+NO_3 oxidation is very similar to the NIST mass

195 spectra of benzaldehyde (C_7H_6O) and 2-hydroxy-1-phenyl ethanone ($C_8H_8O_2$). However, we do not detect

196 the prominent peaks of dimers in the HR-ToF-AMS, which can be explained by instability of dimer under

197 the high collision energy of the instrument.

198 Figure S3a presents the time series of organics and nitrate as measured by HR-ToF-AMS from a typical

199 experiment. Sulfate is used to normalize the decay of organics and nitrate because it is non-volatile and any

200 decrease in sulfate is reflective of particle wall loss and changes in aerosol collection efficiency (CE) in the

201 HR-ToF-AMS (Henry and Donahue, 2012). Organics and nitrate exhibit similar decay trends. However, the

202 situation differs when examining the time series of major organic families relative to sulfate (Figure S3b).

203 Hydrocarbon fragments (C_xH_y Family), C_xH_yO family, and $C_xH_yO_zN$ (z>1) family exhibit similar decay

204 rates, but decrease more rapidly relative to sulfate than C_xH_yON and $C_xH_yO_z$ families. This may indicate

205 that further aerosol aging leads to the formation of more oxidized fragments ($C_xH_yO_z$) (Boyd et al., 2015).

206 This may also suggest that the aging products are more likely to produce C_xH_yON rather than $C_xH_yO_zN$

207 fragments.

208   FIGAERO-CIMS is used to measure speciated particle-phase composition of styrene+NO_3 SOA,

209   including both dimeric and monomeric products. The characteristic SOA mass spectrum from FIGAERO-

210   CIMS (Figure 3a) is categorized according to molecule types: CHO, CHON, and $CHON_2$, each contains

211   compounds with different numbers of carbon atoms (Figure 3b). The SOA composition is dominated by

212   nitrogen-containing compounds, with $C_xH_yO_zN_2$, $C_xH_yO_zN$, and $C_xH_yO_z$ molecules constituting 91.8%,

213   7.4%, and 0.8% of the measured signal, respectively (Figure 3c). Dimers (with carbon numbers C_9 to C_{16})

214   make up 90.9% of the signal, with the majority being $C_{16}H_xO_zN_2$ dimers constituting 89.4% of the total

215   signal. Figure 4 shows the temporal evolution of major particle-phase products, the dominant product is

216      $C_{16}H_{16}N_2O_8$, contributing 88.3% of the total signal. The next most abundant particle-phase product is

217      $C_8H_9NO_4$, which constitutes 4.1% of the total signal. In addition, $C_8H_7NO_4$, $C_8H_9NO_5$, $C_8H_8N_2O_6$, and

218      $C_8H_8N_2O_7$ are major monomeric particle-phase products. $C_{16}H_{14}N_2O_8$, $C_{16}H_{17}NO_7$, $C_{15}H_{13}NO_6$, and

219      $C_{16}H_{13}NO_6$ are major dimeric particle-phase products. It is noted that it is possible that the compounds

220   detected as monomeric species are formed from the thermal decomposition process in the FIGAERO-CIMS

221   (Yang et al., 2021; Kumar et al., 2023; Stark et al., 2017).

222   **3.3. Hydrolysis of styrene-derived organic nitrates**

223   Building on results from our previous study (Wang et al., 2021b), the unique benzene-related skeleton

224   of styrene ONs can facilitate their rapid hydrolysis. Therefore, we conduct experiments with three different

225   chamber RH, including dry (RH<3%), RH~50%, and RH~70% to study the hydrolysis of styrene-derived

226   ONs. Figures S4a illustrate the time series of nitrate measured by HR-ToF-AMS for these different RH

227   systems. Distinct variations are observed in nitrate levels across different chamber RH conditions. The

228   presence of the small amounts of nitrate prior to the commencement of experiments under different RH

229   conditions could potentially result from the uptake of background nitric acid onto aqueous seed particles

230   (McMurry and Grosjean, 1985; Grosjean, 1985; Matsunaga and Ziemann, 2010; Zhang et al., 2014, 2015;

231   Yeh and Ziemann, 2015; La et al., 2016; Nah et al., 2016a; Krechmer et al., 2016; Huang et al., 2018). After

232   N_2O_5 is injected into the chamber, the large increase in nitrate in the higher RH experiments can be attributed

233   to the reactive uptake of N_2O_5 and/or the dissolution of HNO_3 into aqueous aerosols (Takeuchi and Ng,

234   2019), subsequently neutralized by ammonia to form ammonium nitrate. Therefore, to evaluate the extent

235   of particle phase ONs hydrolysis, the contributions of inorganic nitrate ($NO_{3,Inorg}$) and ONs ($NO_{3,Org}$) to the

236   measured nitrate from HR-ToF-AMS need to be separated.

237   We differentiate the contributions of $NO_{3,Inorg}$ and $NO_{3,Org}$ to the measured nitrate based on the method

238   reported in Farmer et al., (2010), as described in Eq. 2.

239      $$x = \frac{(R_{obs}-R_{NH_4NO_3})(1+R_{ON})}{(R_{ON}-R_{NH_4NO_3})(1+R_{obs})}$$ Eq. 2

240   Where R_{NH4NO3} (*i.e.*, NO^+/ NO_2^+ from ammonium nitrate) is derived from the standard ionization

241   efficiency (IE) calibration of HR-ToF-AMS using 300 nm-sized ammonium nitrate particles, and the value

242   is 1.8. The R_{ON} (*i.e.*, NO^+/ NO_2^+ for ONs) value is dependent on the aerosol chemical composition and

243   instrument. The NO^+/ NO_2^+ ratio throughout all the dry experiments remains constant at approximately 4.9,

244   referred to as R_{ON} in this study. The R_{ON}/R_{NH4NO3} ratio (ratio of ratio, RoR) is 2.7, which falls within the

245   range of previous studies with the presence of ONs (Day et al., 2022). The R_{obs} value is 2.8 and 3.8 for

246   experiments with RH ~70% and 50%, corresponding to $NO_{3,Org}$ contributions of 51% and 80%, respectively.

247   Figures S4b and S5 depict the time series of $NO_{3,Org}$ for experiments under different RH. We also compare

248   the $NO_{3,Org}$ measured by HR-ToF-AMS and speciated ONs measured by FIGAERO-CIMS, which show

249   similar trends (Figure S5).

250   Here, we follow the approach reported in our previous work and used $_pON$/OA ratio to evaluate the

251   extent of ON hydrolysis via Eq. 3 (Takeuchi and Ng, 2019; Takeuchi et al., 2024). It is noted that $_pON$ refers

252   to the total mass concentration of particulate ONs, encompassing both the organic and nitrate components

253   of the ON compounds. Similarly, OA represents the total mass concentration of organic aerosols, which

254   includes both nitrated and non-nitrated organic compounds.

255

$$\frac{_pON}{OA} = \left(\frac{NO_{3,org}}{Organic + NO_{3.org}} \right) \times \left(\frac{MW_{_pON}}{MW_{NO_2,ON}} \right) = \left(\frac{\frac{NO_{3,org}}{Organic}}{1 + \frac{NO_{3,Org}}{Organic}} \right) \times \left(\frac{MW_{_pON}}{MW_{NO_2,ON}} \right) \qquad \text{Eq. 3}$$

256   Where MW_{pON} refers to the average molecular weight of $_pON$ estimated from FIGAERTO-CIMS data.

257   Assuming uniform sensitivity among detected species, MW_{pON} is similar across different experiments,

258   within the range of 182.7-184.0 g mol^{-1}. $MW_{NO_2,ON}$ is the molecular weight of the nitrogen-containing

259   moiety of ONs (*i.e.*, NO_2, 46 g mol^{-1}) measured by the HR-ToF-AMS, as discussed in detail in a recent

260   study by Takeuchi et al. (2024).

261   As illustrated in Figure 5a, the time series of $_pON$/OA stabilizes fairly quickly, similar to what we have

262   observed previously for monoterpene systems (Takeuchi and Ng, 2019). This suggests that the hydrolysis

263   lifetime of ONs that undergo hydrolysis is no more than 30 minutes. The hydrolyzable fraction of styrene-

264   derived ONs can be estimated from the difference in $_pON$/OA between dry and RH experiments once the

265   ratio stabilizes. The hydrolyzable fraction is about 52.7-60.6%. The observed hydrolyzable ONs are

266    $C_{16}H_{16}N_2O_8$, $C_8H_7NO_4$, and $C_8H_9NO_4$, as determined by comparing the FIGAERO-CIMS mass spectra

267   under dry and RH 70% conditions (Figure 5b). The non-nitrated organic species (*i.e.*, $C_8H_8O_5$) is enhanced

268   correspondingly due to the hydrolysis of ONs.

269   **4. Discussion**

270   **4.1 SOA yields over a wide range of organic mass loadings**

271   There is no prior study on SOA formation from styrene+NO_3 oxidation, but previous research has

272   reported SOA formation from photolysis, OH-initiated photooxidation, and ozonolysis of styrene (Figure

273   S6). Photolysis of styrene results in the lowest SOA yields, ranging from 1.8%-3.6%, in the presence of

274 29.4 to 202.7 µg/m³ of ΔM_O (Tajuelo et al., 2019b). Different peroxy radical (RO_2) chemistry, controlled

275 by the concentration of NO, influences the SOA formation during OH-initiated photooxidation of styrene.

276 The SOA yields are observed to be 4.0-5.0% with 174.4-348.3 µg/m³ of ΔM_O in conditions where RO_2+NO

277 chemistry dominated (Tajuelo et al., 2019b), and around 2-35 % with 2.8-430 µg/m³ of ΔM_O where

278 RO_2+RO_2 chemistry prevailed (Yu et al., 2022b; Schueneman et al., 2024). Several previous studies have

279 reported that the SOA yields from the ozonolysis of styrene (Ma et al., 2018; Na et al., 2006) are higher

280 than those from OH-initiated photooxidation of styrene under RO_2+NO chemistry, but lower than those

281 under RO_2+RO_2 chemistry. As shown in Figure S6, the SOA yield from the styrene+NO_3 oxidation is higher

282 than in other styrene oxidation systems when ΔM_O is lower than 80 µg/m³.

283 Organic vapor wall loss has been reported to impact SOA yield calculation and can lead to an

284 underestimation of SOA yields by as much as a factor of 4 (McMurry and Grosjean, 1985; Grosjean, 1985;

285 Matsunaga and Ziemann, 2010; Zhang et al., 2014, 2015; Yeh and Ziemann, 2015; La et al., 2016; Nah et

286 al., 2016a; Krechmer et al., 2016; Huang et al., 2018). Therefore, to evaluate the potential effect of organic

287 vapor wall loss on SOA yields in our study, experiments without seed particles are carried out (Exp. 9 and

288 10). As show in Figure S7, the SOA formation from nucleation experiments (without seed particles) is lower

289 than condensation experiments (with seed particles). Zhang et al. (2014) determine that if organic vapor

290 wall loss is significant in chamber experiments, the addition of more seed particles will lead to an increase

291 in SOA yields. The differences in SOA formation between styrene+NO_3 nucleation experiments and

292 condensation experiments suggest the possible impact of organic vapor wall loss. Although particle wall

293 loss is accounted for, the SOA yields reported in Figure 1 and Table 1 could represent the lower limit owing

294 to vapor wall loss, where organic vapors could have partitioned to the chamber wall rather than to the

295 aerosols.

296 To account for the impact of vapor wall loss, we employ the semi-empirical equation (Eq. 1) for SOA

297 yield to correct for vapor wall loss. The correction relies on two assumptions: (1) styrene+NO_3 oxidation

298 yields two major products, and (2) the partition of these major products between gas and particle phases, as

299 well as vapor wall loss is controlled by C* of these products. The detailed procedures and the relevant

300 equations are shown in Supplementary Information (SI). The SOA yields and the SOA yield curve after this

301 correction is shown in Figure 1 and Table S1. The fitted molar yields (α_1 and α_2) are 0.8 and 0.1, and the

302 fitted partitioning coefficients (K_1 and K_2) are 8.1×10^{-4} and 7.5 (corresponding to C* values of 1.2×10^3

303 µg/m³ and 1×10^{-1} µg/m³, respectively) after vapor wall loss correction (R^2=0.991). The vapor wall loss bias

304 factor, defined as the ratio of aerosol mass loadings after correction to those before correction, ranges from

305 1.3 to 3.2. The vapor wall loss bias factor is smaller for the experiments with the higher organic mass

306 loadings, consistent with results reported by Zhang et al. (2014).

307 In styrene+NO_3 oxidation, two products stand out in abundance, $C_8H_9NO_4$ and $C_{16}H_{16}N_2O_8$, which

308   constitute 92.4% of the total particle signal (Figure 3). We utilize two methods to estimate the C^* of

309     $C_8H_9NO_4$ and $C_{16}H_{16}N_2O_8$: the Estimation Program Interface Suite (EPI Suite) method and FIGAERO

310   thermal desorption method (Takeuchi et al., 2022). The C^* of $C_8H_9NO_4$ and $C_{16}H_{16}N_2O_8$, as simulated by

311   EPI Suite, are $1.6 \times 10^3 \, \mu g/m^3$ and $9.0 \times 10^{-1} \, \mu g/m^3$, respectively. The FIGAERO thermal desorption profiles

312   for $C_8H_9NO_4$ and $C_{16}H_{16}N_2O_8$ are shown in Figure S8. The T_{max} of $C_8H_9NO_4$ and $C_{16}H_{16}N_2O_8$ are 24.6 and

313   67.8 ℃, respectively, corresponding to C^* values of 1.1×10^3 and $2 \times 10^{-1} \, \mu g/m^3$. The C^* of $C_8H_9NO_4$ and

314     $C_{16}H_{16}N_2O_8$, estimated by these two methods are similar to those obtained from the semi-empirical equation

315   (Eq. 1). The consistency of the C^* values across different methods supports the applicability of the semi-

316   empirical equation (Eq. 1) proposed in this study for correcting vapor wall loss in SOA yield calculation.

317   **4.2 Proposed formation mechanisms for styrene-derived organic nitrate monomers and dimers**

318   We present the proposed formation mechanisms of major particle-phase products detected by

319   FIGAERTO-CIMS (Figure 6). The formation mechanisms involve two distinct routes to generate the

320   monomeric and dimeric ONs respectively. In monomeric ONs formation pathway (Pathway A): The

321   reaction begins with the addition of a nitrooxy group ($-ONO_2$) onto the double bond of styrene follow by

322   O_2 addition to form a nitrooxy peroxy radical (via R1). This addition is expected to be favored because the

323   NO_3 radical adds to the less substituted carbon atom in the double bond. We also propose the formation

324   mechanism with NO_3 radical adduct to the more substituted carbon atom in the double bond in Figure S9.

325   The nitrooxy peroxy radical can further react with RO_2 or hydroperoxyl radical (HO_2) to produce the styrene

326   hydroxy nitrate ($C_8H_9NO_4$), ketone nitrate ($C_8H_7NO_4$), and peroxy nitrate ($C_8H_9NO_5$) via reactions R2, R3,

327   and R4, respectively. $C_8H_9NO_4$, which is the second most abundant product, has been observed in ambient

328   environments as well. However, it has been assumed to be nitroaromatic compounds ($R-NO_2$, *i.e.*,

329   dimethoxynitrobenzene) instead of aromatic ONs ($R-ONO_2$) (Kong et al., 2021; Wang et al., 2021a;

330   Salvador et al., 2021). $C_8H_9NO_5$ and $C_8H_7NO_4$ are also identified from residential wood-burning boilers

331   and have been suggested to be nitroaromatic compounds (Salvador et al., 2021) formed from the OH-

332   initiated photooxidation of phenolic VOCs in the presence of NO (Vione et al., 2001, 2004; Jenkin et al.,

333   2003; Frka et al., 2016; Vidović et al., 2018). Considering the ambient concentrations of nitroaromatic

334   compounds remain high even at night (Wang et al., 2019), our work suggests that styrene-derived ONs

335   could account for these molecular species in ambient environments, often only attributed to nitroaromatic

336   compounds. Furthermore, the nitrooxy peroxy radical can react with NO_3 radical to produce alkoxyl (RO)

337   radical (via R6). The RO radical can further undergo decomposition to produce benzaldehyde, benzene

338   hydroxy aldehyde, and NO_2 as the byproduct. NO_2 can react with nitrooxy peroxy radical as well through

339   reaction R5 to produce styrene peroxy nitrate ($C_8H_8N_2O_7$). Peroxy nitrate remains unstable at room

340   temperature unless there is a carbonyl group present to induce an electron-withdrawing effect, thereby

341   stabilizing the peroxy nitrooxy group (Yu et al., 2022b). Here, the benzene ring can also stabilize the peroxy

342 nitrooxy group through electron coupling (McMurry, 2012), thus promoting the formation of styrene peroxy

343 nitrate. According to Lewis and Moodie (1996), NO_3 radical can react with the double bond in olefins to

344 produce the ONs containing two nitrooxy groups. We utilize the same mechanism to elucidate the formation

345 of $C_8H_8N_2O_6$ in our work (via R7).

346   The formation of nitrogen-containing dimeric products from aromatic oxidation systems has been

347 observed in laboratory chamber studies (Molteni et al., 2018; Kumar et al., 2023; Mayorga et al., 2021).

348 For example, Kumar et al. (2023) report that dimeric products make up 54.2% of the total particle signal in

349 NO_3 oxidation of an aromatic hydrocarbon mixture, with the majority (42.3%) being $C_xH_yO_zN$ dimers.

350 Nitrated diphenyl ether dimers have been observed from the NO_3 oxidation of phenolic VOCs, as reported

351 by Mayorga et al. (2021). In our work, the predominant dimeric product is $C_{16}H_{16}N_2O_8$, which is generated

352 from RO_2+RO_2 reaction (via R8). Additionally, $C_{16}H_{14}N_2O_8$, $C_{16}H_{17}NO_7$, $C_{15}H_{13}NO_6$, and $C_{16}H_{13}NO_6$ are

353 also major dimeric ONs products observed in the particle phase. Benzaldehyde, ketone nitrate ($C_8H_7NO_4$),

354 and benzene hydroxy aldehyde, can further react with NO_3 radical via reactions R9, R10, and R11 to

355 generate radicals A1, A2, and A3, respectively. A2 and A3 can further react with each other (via R12) to

356 terminate the radical reaction by producing $C_{16}H_{13}NO_6$. Additionally, A3 can react with RO radical from

357 reaction R5 to form $C_{16}H_{14}N_2O_8$ (via R13), while A1 can react with nitrooxy peroxy radical to produce

358 $C_{15}H_{13}NO_6$ (via R14). We propose the formation of $C_{16}H_{17}NO_6$ through the reaction between nitrooxy

359 peroxy radical and styrene (via R15), followed by the $RO_2 + RO_2$ reaction (via R16). It is noted that in this

360 work, we propose formation mechanisms of dimeric compounds based on molecular formulas of the

361 detected species. Further experimental studies and density functional theory work are necessary to confirm

362 the structures and formation of these dimeric compounds.

363 **4.3 Hydrolysis of organic nitrates formed from styrene+NO_3 oxidation**

364   Condensed-phase hydrolysis has been identified as a significant sink for ONs, evidenced by substantial

365 ON uptake to aerosols and the reported short hydrolysis lifetimes (Pye et al., 2015; Fisher et al., 2016; Zare

366 et al., 2019; Vasquez et al., 2021). Recent studies have reported experimentally constrained parameters for

367 the hydrolysis of biogenic ONs derived from monoterpene or isoprene, through chamber or bulk solution

368 experiments (Takeuchi and Ng, 2019; Morales et al., 2021; Hu et al., 2011; Darer et al., 2011; Jacobs et al.,

369 2014; Rindelaub et al., 2016; Vasquez et al., 2021; Wang et al., 2021b). Studies using bulk solutions to

370 exam hydrolysis of ONs with specific structures have demonstrated that the number of alkyl substitutions,

371 functional groups, and carbon skeletons are three important factors controlling hydrolysis rates (Wang et

372 al., 2021b). Therefore, the hydrolysis lifetimes of biogenic ONs can be as fast as seconds or minutes, or as

373 stable as several days without observable hydrolysis, depending on the structures of the ONs. Unlike bulk

374 solutions, which only involve aqueous solutions, chamber experiments can simulate the hydrolysis of ONs

375 formed from VOC oxidations in aerosol water. In Takeuchi and Ng (2019), the ON hydrolysis lifetimes are

376 determined to be less than 30 minutes for NO_3 oxidation and OH-initiated photooxidation of α-pinene and

377 β-pinene systems. The hydrolysis lifetime of ONs formed from OH-initiated photooxidation of β-ocimene

378 has been found to be pH-dependent, 51 (±13) minutes at a pH of 4 and 24 (±3) minutes at a pH of 2.5

379 (Morales et al., 2021).

380 There is limited study on the hydrolysis of anthropogenic ONs. Only one study reported the hydrolysis

381 lifetime of ONs resulting from OH-initiated photooxidation of 1,2,4-trimethylbenzene to be 6 hours (Liu et

382 al., 2012). The extended hydrolysis lifetime of ONs from this system can be explained by the cleavage of

383 the benzene ring, which disrupts the delocalized π orbitals. In this study, we determine that the hydrolysis

384 lifetime for ONs from styrene+NO_3 oxidation is no more than 30 minutes. Based on our previous work with

385 bulk solutions (Wang et al., 2021b), we propose that the benzene-related skeleton of aromatic ONs, which

386 contains three delocalized π orbitals, can lead to rapid hydrolysis. This is because the delocalized π orbitals

387 enhance the hyperconjugation effect and stabilize the carbocation, thereby decrease the hydrolysis lifetimes

388 of ONs (Wang et al., 2021b). This mechanism helps explain the short hydrolysis lifetimes observed in this

389 work.

390 The fraction of hydrolyzable ONs is crucial for understanding the role of hydrolysis as a loss

391 mechanism for ONs and NO_x. Takeuchi and Ng (2019) reported that the hydrolysable fraction of ONs from

392 the NO_3 oxidation and OH-initiated photooxidation of α-pinene and β-pinene systems range from 9-36%.

393 However, more than 50% of the ONs resulting from the OH-initiated photooxidation of 1,2,4-

394 trimethylbenzene are hydrolyzable (Liu et al., 2012). In our study, we observe that the fraction of

395 hydrolyzed styrene-derived ONs ranges from 52.7% to 60.6%. Overall, while research on the fraction of

396 hydrolyzable ONs is still limited, these findings so far indicate that the hydrolyzable fraction of ONs

397 resulting from the oxidation of aromatic VOCs are larger than those from biogenic VOCs. The difference

398 can likely be explained by the fact that only ONs with specific chemical structures, particularly tertiary

399 nitrates in biogenic VOCs oxidation systems, are susceptible to hydrolysis. In contrast, a large fraction of

400 aromatic ONs features structures with delocalized π orbitals, which facilitate hydrolysis.

401 **5. Atmospheric implications**

402 To the best of our knowledge, this study is the first to demonstrate the formation of SOA and particulate

403 ONs from styrene+NO_3 oxidation. We systematically carry out a series of chamber experiments with initial

404 styrene concentrations ranging from 9.5 to 155.2 ppb under dry and humid conditions at room temperature.

405 The resulting SOA yields range from 4.5% to 16.1% with the aerosol mass loadings of 1.9 to 107.4 μg/m³.

406 It is known that the loss of organic vapors to the chamber wall can lead to underestimation of SOA yields.

407 For instance, Zhang et al. (2014) compare the results from a statistical oxidation model and experimental

408 observations and determine that the correction factor for SOA yields to range from 2.1 to 4.2. Here, we use

409 a semi-empirical model that incorporates the gas-to-particle partitioning of two semi-volatile products to

410 correct for the effect of vapor wall loss on SOA yields, the correction factor is found to range from 1.3 to

411 3.2, consistent with previous studies (Zhang et al., 2014). By applying the correction factor derived in this

412 work, the corrected SOA yields range from 14.0% to 22.1% with the aerosol mass loadings of 5.9 to 147.6

413 $\mu g/m^3$. The yields obtained in this study provide the basis to determine the contributions of styrene+NO_3

414 chemistry to SOA formation. Styrene has been detected at the ppb levels in ambient atmosphere and has a

415 high emission factor from biomass burning, with typical abundance ranging from 0.06 to 45 ppb (Cho et

416 al., 2014; Tuazon et al., 1993; Yu et al., 2019; Koss et al., 2018). These are in the range of our experiments,

417 corresponding to the formation of up to 32.5 $\mu g/m^3$ of SOA with the vapor wall loss correction. Our results

418 serve as fundamental inputs for parameterizing SOA formation from styrene in atmospheric models.

419   We examine the chemical composition of SOA and propose formation mechanisms for the major

420 monomeric and dimeric ON products detected in the particle phase. We find that dimeric products constitute

421 90.9% of the signal, while monomeric products account for only 9.1%. Previous studies have identified

422 nitroaromatic compounds (R-NO_2) as the nitrogen-containing products from aromatic VOCs in ambient

423 conditions (Kong et al., 2021; Wang et al., 2021a; Salvador et al., 2021). Our work introduces an alternative

424 perspective, suggesting that ONs could also be nitrogen-containing products from the oxidation of aromatic

425 VOCs in the atmosphere. Dimeric nitrogen-containing compounds from the oxidation of aromatic VOCs

426 (*e.g.*, toluene, p-xylene, ethylbenzene, 1,3,5-trimethylbenzene, phenol, cresol, 2,6-dimethylphenol, and etc.)

427 have been observed in chamber experiments (Molteni et al., 2018; Kumar et al., 2023; Mayorga et al., 2021).

428 Here, based on speciated molecular level characterization of SOA, we are able to propose the chemical

429 structures and formation mechanisms of dimeric ON products for the first time. Besides the common

430 RO_2+RO_2 pathway, we also suggest that other radical chain termination reactions, such as RO+R or R+R,

431 could explain the formation of the major dimeric ONs. Further density functional theory calculations and

432 experimental work are needed to provide additional evidence for our proposed mechanisms. In contrast to

433 chamber experiments, the detection of dimeric nitrogen-containing compounds derived from aromatics is

434 rare in field campaigns. Ye et al. (2021) observe $C_{\geqslant 19}H_yO_zN_{1-2}$ compounds in ambient aerosols in Shenzhen,

435 China by FIGAERO-CIMS, exhibiting a ring and double-bond equivalence (RDBE) exceeding 10 and an

436 aromaticity equivalent (Xc) surpassing 2.70 (Yassine et al., 2014; Wang et al., 2017). These compounds can

437 be considered as aromatic ONs (Table S2). Considering the difference between controlled laboratory

438 experiments and the complexity of ambient environments, it will be intriguing to explore why dimeric ONs

439 derived from aromatic compounds are rarely observed in the field.

440   In this study, we observe that the hydrolysis lifetime of styrene-derived ONs (about 52.7 to 60.6% of

441 total ONs) is no more than 30 minutes. This finding supports our previous assumptions about the

442 relationship between hydrolysis lifetimes and the molecular structures of ONs (Wang et al., 2021b). The

443 unique delocalized π orbitals provided by the benzene-related skeleton of styrene ONs can stabilize the

444 carbocation, thereby promoting hydrolysis. The hydrolysis lifetime observed for ONs generated from
445 styrene+NO$_3$ oxidation can serve as experimentally constrained parameter for modeling hydrolysis of
446 aromatic ONs in general. For example, not only styrene-derived ONs but also other aromatic ONs such as
447 furan or methylfuran ONs (Joo et al., 2019), despite lacking benzene ring, have the potential to undergo
448 rapid hydrolysis due to the presence of delocalized π orbitals. The hydrolysis lifetimes are crucial for
449 regional and global chemical transport models to accurately assess the impacts of hydrolysis of aromatic
450 ONs on the nitrogen budget and subsequent ozone formation.
451

452 **Data availability.**
453 The chamber experiment data are available online at the Index of Chamber Atmospheric Research in the
454 United States (ICARUS, https://icarus.ucdavis.edu/).
455

456 **Supporting Information**
457 The Supporting Information is available free of charge at: https:// /acp.copernicus.org. Additional details
458 on volatility calibration, HR-ToF-AMS and FIGAERO-CIMS mass spectra of SOA from styrene+NO$_3$
459 oxidation, representative product distribution, time series data from HR-ToF-AMS for different RH
460 experiments, literature review of previous styrene oxidation studies, method for correcting vapor wall loss
461 when determining SOA yields, and other proposed mechanisms for the major particle-phase products.
462

463 **Author contributions**
464 YW and NLN designed the research. YW conducted the experiments. YW, XZ, and NLN interpreted the
465 data and wrote the paper. YL conducted volatility calibration and YH helped with vapor wall loss correction.
466 All the authors discussed the results and commented on the paper.
467

468 **Competing interests.**
469 The authors declare that they have no conflict of interest.
470

482

References:

484 Alfarra, M. R., Paulsen, D., Gysel, M., Garforth, A. A., Dommen, J., Prévôt, A. S. H., Worsnop, D. R.,
485   Baltensperger, U., and Coe, H.: A mass spectrometric study of secondary organic aerosols formed
486   from the photooxidation of anthropogenic and biogenic precursors in a reaction chamber, Atmos.
487   Chem. Phys., 6, 5279–5293, https://doi.org/10.5194/acp-6-5279-2006, 2006.

488 Atkinson, R. and Aschmann, S. M.: Kinetics of the reactions of acenaphthene and acenaphthylene and
489   structurally-related aromatic compounds with OH and NO3 radicals, N2O5 and O3 at 296 ± 2 K, Int.
490   J. Chem. Kinet., 20, 513–539, https://doi.org/10.1002/kin.550200703, 1988.

491 Bahreini, R., Keywood, M. D., Ng, N. L., Varutbangkul, V., Gao, S., Flagan, R. C., Seinfeld, J. H., Worsnop,
492   D. R., and Jimenez, J. L.: Measurements of secondary organic aerosol from oxidation of cycloalkenes,
493   terpenes, and m-xylene using an aerodyne aerosol mass spectrometer, Environ. Sci. Technol., 39,
494   5674–5688, https://doi.org/10.1021/es048061a, 2005.

495 Boyd, C. M., Sanchez, J., Xu, L., Eugene, A. J., Nah, T., Tuet, W. Y., Guzman, M. I., and Ng, N. L.:
496   Secondary organic aerosol formation from the β-pinene+NO3 system: Effect of humidity and peroxy
497   radical fate, Atmos. Chem. Phys., 15, 7497–7522, https://doi.org/10.5194/acp-15-7497-2015, 2015.

498 Boyd, C. M., Nah, T., Xu, L., Berkemeier, T., and Ng, N. L.: Secondary Organic Aerosol (SOA) from
499   Nitrate Radical Oxidation of Monoterpenes: Effects of Temperature, Dilution, and Humidity on
500   Aerosol Formation, Mixing, and Evaporation, Environ. Sci. Technol., 51, 7831–7841,
501   https://doi.org/10.1021/acs.est.7b01460, 2017.

502 Cabrera-Perez, D., Taraborrelli, D., Sander, R., and Pozzer, A.: Global atmospheric budget of simple
503   monocyclic aromatic compounds, Atmos. Chem. Phys., 16, 6931–6947, https://doi.org/10.5194/acp-
504   16-6931-2016, 2016.

505 Calvert, J. G., Atkinson, R., Becker, K. H., Kamens, R. M., Seinfeld, J. H., Wallington, T. H., and Yarwood,
506   G.: The Mechanisms of Atmospheric Oxidation of the Aromatic Hydrocarbons, Oxford University
507   Press, 2002.

508 Canagaratna, M. R., Jimenez, J. L., Kroll, J. H., Chen, Q., Kessler, S. H., Massoli, P., Hildebrandt Ruiz, L.,
509   Fortner, E., Williams, L. R., Wilson, K. R., Surratt, J. D., Donahue, N. M., Jayne, J. T., and Worsnop,
510   D. R.: Elemental ratio measurements of organic compounds using aerosol mass spectrometry:

511   Characterization, improved calibration, and implications, Atmos. Chem. Phys., 15, 253–272,

512   https://doi.org/10.5194/acp-15-253-2015, 2015.

513   Chen, T., Chu, B., Ma, Q., Zhang, P., Liu, J., and He, H.: Effect of relative humidity on SOA formation

514   from aromatic hydrocarbons: Implications from the evolution of gas- and particle-phase species, Sci.

515   Total Environ., 773, 145015, https://doi.org/10.1016/j.scitotenv.2021.145015, 2021.

516   Chen, Y., Takeuchi, M., Nah, T., Xu, L., Canagaratna, M. R., Stark, H., Baumann, K., Canonaco, F., Prevot,

517   A. S. H., Gregory Huey, L., Weber, R. J., and Ng, N. L.: Chemical characterization of secondary

518   organic aerosol at a rural site in the southeastern US: Insights from simultaneous high-resolution time-

519   of-flight aerosol mass spectrometer (HR-ToF-AMS) and FIGAERO chemical ionization mass

520   spectrometer (CIMS) measur, Atmos. Chem. Phys., 20, 8421–8440, https://doi.org/10.5194/acp-20-

521   8421-2020, 2020.

522   Cho, J., Roueintan, M., and Li, Z.: Kinetic and dynamic investigations of oh reaction with styrene, J. Phys.

523   Chem. A, 118, 9460–9470, https://doi.org/10.1021/jp501380j, 2014.

524   Darer, A. I., Cole-Filipiak, N. C., O'Connor, A. E., and Elrod, M. J.: Formation and stability of

525   atmospherically relevant isoprene-derived organosulfates and organonitrates, Environ. Sci. Technol.,

526   45, 1895–1902, https://doi.org/10.1021/es103797z, 2011.

527   Day, D. A., Campuzano-jost, P., Nault, B. A., Palm, B. B., Hu, W., Martin, S. T., and Jimenez, J. L.: A

528   systematic re-evaluation of methods for quantification of bulk particle-phase organic nitrates using

529   real-time aerosol mass spectrometry, Atmos. Meas. Tech., 15, 459–483, 2022.

530   DeCarlo, P. F., Kimmel, J. R., Trimborn, A., Northway, M. J., Jayne, J. T., Aiken, A. C., Gonin, M., Fuhrer,

531   K., Horvath, T., Docherty, K. S., Worsnop, D. R., and Jimenez, J. L.: Field-deployable, high-resolution,

532   time-of-flight aerosol mass spectrometer, Anal. Chem., 78, 8281–8289,

533   https://doi.org/10.1021/ac061249n, 2006.

534   Decker, Z. C. J., Robinson, M. A., Barsanti, K. C., Bourgeois, I., Coggon, M. M., Digangi, J. P., Diskin, G.

535   S., Flocke, F. M., Franchin, A., Fredrickson, C. D., Gkatzelis, G. I., Hall, S. R., Halliday, H., Holmes,

536   C. D., Huey, L. G., Lee, Y. R., Lindaas, J., Middlebrook, A. M., Montzka, D. D., Moore, R., Neuman,

537   J. A., Nowak, J. B., Palm, B. B., Peischl, J., Piel, F., Rickly, P. S., Rollins, A. W., Ryerson, T. B.,

538   Schwantes, R. H., Sekimoto, K., Thornhill, L., Thornton, J. A., Tyndall, G. S., Ullmann, K., Van Rooy,

539   P., Veres, P. R., Warneke, C., Washenfelder, R. A., Weinheimer, A. J., Wiggins, E., Winstead, E.,

540   Wisthaler, A., Womack, C., and Brown, S. S.: Nighttime and daytime dark oxidation chemistry in

541   wildfire plumes: An observation and model analysis of FIREX-AQ aircraft data, Atmos. Chem. Phys.,

542   21, 16293–16317, https://doi.org/10.5194/acp-21-16293-2021, 2021.

543   Farmer, D. K., Matsunaga, A., Docherty, K. S., Surratt, J. D., Seinfeld, J. H., Ziemann, P. J., and Jimenez,

544   J. L.: Response of an aerosol mass spectrometer to organonitrates and organosulfates and implications

545   for atmospheric chemistry, Proc. Natl. Acad. Sci. U. S. A., 107, 6670–6675,
546   https://doi.org/10.1073/pnas.0912340107, 2010.

547   Fisher, J. A., Jacob, D. J., Travis, K. R., Kim, P. S., Marais, E. A., Miller, C. C., Yu, K., Zhu, L., Yantosca,
548   R. M., Sulprizio, M. P., Mao, J., Wennberg, P. O., Crounse, J. D., Teng, A. P., Nguyen, T. B., Clair,
549   J. M. S., Cohen, R. C., Romer, P., Nault, B. A., Wooldridge, P. J., Jimenez, J. L., Campuzano-Jost, P.,
550   Day, D. A., Hu, W., Shepson, P. B., Xiong, F., Blake, D. R., Goldstein, A. H., Misztal, P. K., Hanisco,
551   T. F., Wolfe, G. M., Ryerson, T. B., Wisthaler, A., and Mikoviny, T.: Organic nitrate chemistry and
552   its implications for nitrogen budgets in an isoprene- and monoterpene-rich atmosphere: Constraints
553   from aircraft (SEAC4RS) and ground-based (SOAS) observations in the Southeast US, 5969–5991
554   pp., https://doi.org/10.5194/acp-16-5969-2016, 2016.

555   Frka, S., Šala, M., Kroflič, A., Huš, M., Čusak, A., and Grgić, I.: Quantum Chemical Calculations Resolved
556   Identification of Methylnitrocatechols in Atmospheric Aerosols, Environ. Sci. Technol., 50, 5526–
557   5535, https://doi.org/10.1021/acs.est.6b00823, 2016.

558   Grosjean, D.: Wall Loss of Gaseous Pollutants in Outdoor Teflon Chambers, Environ. Sci. Technol., 19,
559   1059–1065, https://doi.org/10.1021/es00141a006, 1985.

560   Helal, S. F. and Elshafy, W. S.: Health hazards among workers in plastic industry, Toxicol. Ind. Health, 29,
561   812–819, https://doi.org/10.1177/0748233712442728, 2012.

562   Henry, K. M. and Donahue, N. M.: Photochemical aging of α-pinene secondary organic aerosol: Effects of
563   OH radical sources and photolysis, J. Phys. Chem. A, 116, 5932–5940,
564   https://doi.org/10.1021/jp210288s, 2012.

565   Hu, K. S., Darer, A. I., and Elrod, M. J.: Thermodynamics and kinetics of the hydrolysis of atmospherically
566   relevant organonitrates and organosulfates, Atmos. Chem. Phys., 11, 8307–8320,
567   https://doi.org/10.5194/acp-11-8307-2011, 2011.

568   Huang, Y., Zhao, R., Charan, S. M., Kenseth, C. M., Zhang, X., and Seinfeld, J. H.: Unified Theory of
569   Vapor-Wall Mass Transport in Teflon-Walled Environmental Chambers, Environ. Sci. Technol., 52,
570   2134–2142, https://doi.org/10.1021/acs.est.7b05575, 2018.

571   Jacobs, M. I., Burke, W. J., and Elrod, M. J.: Kinetics of the reactions of isoprene-derived hydroxynitrates:
572   Gas phase epoxide formation and solution phase hydrolysis, Atmos. Chem. Phys., 14, 8933–8946,
573   https://doi.org/10.5194/acp-14-8933-2014, 2014.

574   Jenkin, M. E., Saunders, S. M., Wagner, V., and Pilling, M. J.: Protocol for the development of the Master
575   Chemical Mechanism, MCM v3 (Part B): Tropospheric degradation of aromatic volatile organic
576   compounds, Atmos. Chem. Phys., 3, 181–193, https://doi.org/10.5194/acp-3-181-2003, 2003.

577   Jiang, H., Cai, J., Feng, X., Chen, Y., Wang, L., Jiang, B., Liao, Y., Li, J., Zhang, G., Mu, Y., and Chen, J.:
578   Aqueous-Phase Reactions of Anthropogenic Emissions Lead to the High Chemodiversity of

https://doi.org/10.5194/egusphere-2024-3849
Preprint. Discussion started: 13 December 2024
© Author(s) 2024. CC BY 4.0 License.

579   Atmospheric Nitrogen-Containing Compounds during the Haze Event, Environ. Sci. Technol., 57,
580   16500–16511, https://doi.org/10.1021/acs.est.3c06648, 2023.

581 Joo, T., Rivera-Rios, J. C., Takeuchi, M., Alvarado, M. J., and Ng, N. L.: Secondary Organic Aerosol
582   Formation from Reaction of 3-Methylfuran with Nitrate Radicals, ACS Earth Sp. Chem., 3, 922–934,
583   https://doi.org/10.1021/acsearthspacechem.9b00068, 2019.

584 Knighton, W. B., Herndon, S. C., Wood, E. C., Fortner, E. C., Onasch, T. B., Wormhoudt, J., Kolb, C. E.,
585   Lee, B. H., Zavala, M., Molina, L., and Jones, M.: Detecting fugitive emissions of 1,3-butadiene and
586   styrene from a petrochemical facility: An application of a mobile laboratory and a modified proton
587   transfer reaction mass spectrometer, Ind. Eng. Chem. Res., 51, 12706–12711,
588   https://doi.org/10.1021/ie202794j, 2012.

589 Kong, X., Salvador, C. M., Carlsson, S., Pathak, R., Davidsson, K. O., Le Breton, M., Gaita, S. M., Mitra,
590   K., Hallquist, Å. M., Hallquist, M., and Pettersson, J. B. C.: Molecular characterization and optical
591   properties of primary emissions from a residential wood burning boiler, Sci. Total Environ., 754,
592   142143, https://doi.org/10.1016/j.scitotenv.2020.142143, 2021.

593 Koss, A. R., Sekimoto, K., Gilman, J. B., Selimovic, V., Coggon, M. M., Zarzana, K. J., Yuan, B., Lerner,
594   B. M., Brown, S. S., Jimenez, J. L., Krechmer, J., Roberts, J. M., Warneke, C., Yokelson, R. J., and
595   De Gouw, J.: Non-methane organic gas emissions from biomass burning: Identification, quantification,
596   and emission factors from PTR-ToF during the FIREX 2016 laboratory experiment, Atmos. Chem.
597   Phys., 18, 3299–3319, https://doi.org/10.5194/acp-18-3299-2018, 2018.

598 Krechmer, J. E., Pagonis, D., Ziemann, P. J., and Jimenez, J. L.: Quantification of Gas-Wall Partitioning in
599   Teflon Environmental Chambers Using Rapid Bursts of Low-Volatility Oxidized Species Generated
600   in Situ, Environ. Sci. Technol., 50, 5757–5765, https://doi.org/10.1021/acs.est.6b00606, 2016.

601 Kumar, V., Slowik, J. G., Baltensperger, U., Prevot, A. S. H., and Bell, D. M.: Time-Resolved Molecular
602   Characterization of Secondary Organic Aerosol Formed from OH and NO3 Radical Initiated
603   Oxidation of a Mixture of Aromatic Precursors, Environ. Sci. Technol., 57, 11572–11582,
604   https://doi.org/10.1021/acs.est.3c00225, 2023.

605 La, Y. S., Camredon, M., Ziemann, P. J., Valorso, R., Matsunaga, A., Lannuque, V., Lee-Taylor, J., Hodzic,
606   A., Madronich, S., and Aumont, B.: Impact of chamber wall loss of gaseous organic compounds on
607   secondary organic aerosol formation: Explicit modeling of SOA formation from alkane and alkene
608   oxidation, Atmos. Chem. Phys., 16, 1417–1431, https://doi.org/10.5194/acp-16-1417-2016, 2016.

609 Lewis, R. J. and Moodie, R. B.: Nitration of styrenes by dinitrogen pentoxide in dichloromethane, J. Chem.
610   Soc. Perkin Trans. 2, 1315–1320, 1996.

611 Lin, C., Huang, R. J., Duan, J., Zhong, H., and Xu, W.: Primary and Secondary Organic Nitrate in Northwest
612   China: A Case Study, Environ. Sci. Technol. Lett., 8, 947–953,

613   https://doi.org/10.1021/acs.estlett.1c00692, 2021.

614   Liu, S., Shilling, J. E., Song, C., Hiranuma, N., Zaveri, R. A., and Russell, L. M.: Hydrolysis of

615   organonitrate functional groups in aerosol particles, Aerosol Sci. Technol., 46, 1359–1369,

616   https://doi.org/10.1080/02786826.2012.716175, 2012.

617   Liu, S., Liu, X., Wang, Y., Zhang, S., Wu, C., Du, W., and Wang, G.: Effect of NOx and RH on the

618   secondary organic aerosol formation from toluene photooxidation, J. Environ. Sci. (China), 114, 1–9,

619   https://doi.org/10.1016/j.jes.2021.06.017, 2022.

620   Lopez-Hilfiker, F. D., Mohr, C., Ehn, M., Rubach, F., Kleist, E., Wildt, J., Mentel, T. F., Lutz, A., Hallquist,

621   M., Worsnop, D., and Thornton, J. A.: A novel method for online analysis of gas and particle

622   composition: Description and evaluation of a filter inlet for gases and AEROsols (FIGAERO), Atmos.

623   Meas. Tech., 7, 983–1001, https://doi.org/10.5194/amt-7-983-2014, 2014.

624   Lu, B., Meng, X., Dong, S., Zhang, Z., Liu, C., Jiang, J., Herrmann, H., and Li, X.: High-resolution mapping

625   of regional VOCs using the enhanced space-time extreme gradient boosting machine (XGBoost) in

626   Shanghai, Sci. Total Environ., 905, 167054, https://doi.org/10.1016/j.scitotenv.2023.167054, 2023a.

627   Lu, Y., Ma, Y., Huang, D. D., Lou, S., Jing, S., Gao, Y., Wang, H., Zhang, Y., Chen, H., Chang, Y., Yan,

628   N., Chen, J., George, C., Riva, M., and Huang, C.: Unambiguous identification of N-containing

629   oxygenated organic molecules using a chemical-ionization Orbitrap (CI-Orbitrap) in an eastern

630   Chinese megacity, Atmos. Chem. Phys., 23, 3233–3245, https://doi.org/10.5194/acp-23-3233-2023,

631   2023b.

632   Ma, Q., Lin, X., Yang, C., Long, B., Gai, Y., and Zhang, W.: The influences of ammonia on aerosol

633   formation in the ozonolysis of styrene: Roles of criegee intermediate reactions, R. Soc. Open Sci., 5,

634   172171–172183, https://doi.org/10.1098/rsos.172171, 2018.

635   Matsunaga, A. and Ziemann, P. J.: Gas-wall partitioning of organic compounds in a teflon film chamber

636   and potential effects on reaction product and aerosol yield measurements, Aerosol Sci. Technol., 44,

637   881–892, https://doi.org/10.1080/02786826.2010.501044, 2010.

638   Mayorga, R. J., Zhao, Z., and Zhang, H.: Formation of secondary organic aerosol from nitrate radical

639   oxidation of phenolic VOCs: Implications for nitration mechanisms and brown carbon formation,

640   Atmos. Environ., 244, 117910, https://doi.org/10.1016/j.atmosenv.2020.117910, 2021.

641   McLafferty, F. W. and Turecek, F.: Interpretation Of Mass Spectra, University Science Books, 1993.

642   McMurry, J.: Organic Chemistry, Brooks/Cole Cengage Learning, 2012.

643   McMurry, P. H. and Grosjean, D.: Gas and Aerosol Wall Losses in Teflon Film Smog Chambers, Environ.

644   Sci. Technol., 19, 1176–1182, https://doi.org/10.1021/es00142a006, 1985.

645   Molteni, U., Bianchi, F., Klein, F., El Haddad, I., Frege, C., Rossi, M. J., Dommen, J., and Baltensperger,

646   U.: Formation of highly oxygenated organic molecules from aromatic compounds, Atmos. Chem.

647   Phys., 18, 1909–1921, https://doi.org/10.5194/acp-18-1909-2018, 2018.

648 Morales, A. C., Jayarathne, T., Slade, J. H., Laskin, A., and Shepson, P. B.: The production and hydrolysis
649   of organic nitrates from OH radical oxidation of β-ocimene, Atmos. Chem. Phys., 21, 129–145,
650   https://doi.org/10.5194/acp-21-129-2021, 2021.

651 Na, K., Song, C., and Cocker, D. R.: Formation of secondary organic aerosol from the reaction of styrene
652   with ozone in the presence and absence of ammonia and water, Atmos. Environ., 40, 1889–1900,
653   https://doi.org/10.1016/j.atmosenv.2005.10.063, 2006.

654 Nah, T., Mcvay, R. C., Zhang, X., Boyd, C. M., Seinfeld, J. H., and Ng, N. L.: Influence of seed aerosol
655   surface area and oxidation rate on vapor wall deposition and SOA mass yields : a case study with α -
656   pinene ozonolysis, Atmos. Chem. Phys., 16, 9361–9379, https://doi.org/10.5194/acp-16-9361-2016,
657   2016a.

658 Nah, T., Sanchez, J., Boyd, C. M., and Ng, N. L.: Photochemical Aging of α-pinene and β-pinene Secondary
659   Organic Aerosol formed from Nitrate Radical Oxidation, Environ. Sci. Technol., 50, 222–231,
660   https://doi.org/10.1021/acs.est.5b04594, 2016b.

661 Nah, T., McVay, R. C., Pierce, J. R., Seinfeld, J. H., and Ng, N. L.: Constraining uncertainties in particle-
662   wall deposition correction during SOA formation in chamber experiments, Atmos. Chem. Phys., 17,
663   2297–2310, https://doi.org/10.5194/acp-17-2297-2017, 2017.

664 Ng, L. N., Brown, S. S., Archibald, A. T., Atlas, E., Cohen, R. C., Crowley, J. N., Day, D. A., Donahue, N.
665   M., Fry, J. L., Fuchs, H., Griffin, R. J., Guzman, M. I., Herrmann, H., Hodzic, A., Iinuma, Y., Kiendler-
666   Scharr, A., Lee, B. H., Luecken, D. J., Mao, J., McLaren, R., Mutzel, A., Osthoff, H. D., Ouyang, B.,
667   Picquet-Varrault, B., Platt, U., Pye, H. O. T., Rudich, Y., Schwantes, R. H., Shiraiwa, M., Stutz, J.,
668   Thornton, J. A., Tilgner, A., Williams, B. J., and Zaveri, R. A.: Nitrate radicals and biogenic volatile
669   organic compounds: Oxidation, mechanisms, and organic aerosol, Atmos. Chem. Phys., 17, 2103–
670   2162, https://doi.org/10.5194/acp-17-2103-2017, 2017.

671 Ng, N. L., Kwan, A. J., Surratt, J. D., Chan, A. W. H., Chhabra, P. S., Sorooshian, A., Pye, H. O. T., Crounse,
672   J. D., Wennberg, P. O., Flagan, R. C., and Seinfeld, J. H.: Secondary organic aerosol (SOA) formation
673   from reaction of isoprene with nitrate radicals (NO3), Atmos. Chem. Phys., 8, 4117–4140,
674   https://doi.org/10.5194/acp-8-4117-2008, 2008.

675 Odum, J. R., Hoffmann, T., Bowman, F., Collins, D., Flagan, R. C., and Seinfeld, J. H.: Gas/particle
676   partitioning and secondary organic aerosol yields, Environ. Sci. Technol., 30, 2580–2585,
677   https://doi.org/10.1021/es950943+, 1996.

678 Odum, J. R., Jungkamp, T. P. W., Griffin, R. J., Flagan, R. C., and Seinfeld, J. H.: The Atmospheric
679   Aerosol-Forming Potential of Whole Gasoline Vapor, Science (80-.)., 276, 96–99,
680   https://doi.org/10.1126/science.276.5309.96, 1997.

681   Okada, Y., Nakagoshi, A., Tsurukawa, M., Matsumura, C., Eiho, J., and Nakano, T.: Environmental risk
682   assessment and concentration trend of atmospheric volatile organic compounds in Hyogo Prefecture,
683   Japan, Environ. Sci. Pollut. Res., 19, 201–213, https://doi.org/10.1007/s11356-011-0550-0, 2012.

684   Orel, A. E., Peterson, T. W., and Seinfeld, J. H.: Nitrate Formation in Atmospheric Aerosols., Environ. Sci.
685   Technol., 18, 410–411, https://doi.org/10.1021/es60142a016, 1978.

686   Le Person, A., Eyglunent, G., Daële, V., Mellouki, A., and Mu, Y.: The near UV absorption cross-sections
687   and the rate coefficients for the ozonolysis of a series of styrene-like compounds, J. Photochem.
688   Photobiol. A Chem., 195, 54–63, https://doi.org/10.1016/j.jphotochem.2007.09.006, 2008.

689   Pye, H. O. T., Luecken, D. J., Xu, L., Boyd, C. M., Ng, N. L., Baker, K. R., Ayres, B. R., Bash, J. O.,
690   Baumann, K., Carter, W. P. L., Edgerton, E., Fry, J. L., Hutzell, W. T., Schwede, D. B., and Shepson,
691   P. B.: Modeling the Current and Future Roles of Particulate Organic Nitrates in the Southeastern
692   United States, Environ. Sci. Technol., 49, 14195–14203, https://doi.org/10.1021/acs.est.5b03738,
693   2015.

694   Rindelaub, J. D., Borca, C. H., Hostetler, M. A., Slade, J. H., Lipton, M. A., Slipchenko, L. V., and Shepson,
695   P. B.: The acid-catalyzed hydrolysis of an α-pinene-derived organic nitrate: Kinetics, products,
696   reaction mechanisms, and atmospheric impact, Atmos. Chem. Phys., 16, 15425–15432,
697   https://doi.org/10.5194/acp-16-15425-2016, 2016.

698   Salvador, C. M. G., Tang, R., Priestley, M., Li, L., Tsiligiannis, E., Le Breton, M., Zhu, W., Zeng, L., Wang,
699   H., Yu, Y., Hu, M., Guo, S., and Hallquist, M.: Ambient nitro-aromatic compounds-biomass burning
700   versus secondary formation in rural China, Atmos. Chem. Phys., 21, 1389–1406,
701   https://doi.org/10.5194/acp-21-1389-2021, 2021.

702   Schueneman, M. K., Day, D. A., Peng, Z., Pagonis, D., Jenks, O. J., de Gouw, J. A., and Jimenez, J. L.:
703   Secondary Organic Aerosol Formation from the OH Oxidation of Phenol, Catechol, Styrene, Furfural,
704   and   Methyl   Furfural,   ACS   Earth   Sp.   Chem.,   8,   1179–1192,
705   https://doi.org/10.1021/acsearthspacechem.3c00361, 2024.

706   Stark, H., Yatavelli, R. L. N., Thompson, S. L., Kang, H., Krechmer, J. E., Kimmel, J. R., Palm, B. B., Hu,
707   W., Hayes, P. L., Day, D. A., Campuzano-Jost, P., Canagaratna, M. R., Jayne, J. T., Worsnop, D. R.,
708   and Jimenez, J. L.: Impact of Thermal Decomposition on Thermal Desorption Instruments: Advantage
709   of Thermogram Analysis for Quantifying Volatility Distributions of Organic Species, Environ. Sci.
710   Technol., 51, 8491–8500, https://doi.org/10.1021/acs.est.7b00160, 2017.

711   Sun, J., Wu, F., Hu, B., Tang, G., Zhang, J., and Wang, Y.: VOC characteristics, emissions and
712   contributions to SOA formation during hazy episodes, Atmos. Environ., 141, 560–570,
713   https://doi.org/10.1016/j.atmosenv.2016.06.060, 2016.

714   Tajuelo, M., Bravo, I., Rodríguez, A., Aranda, A., Díaz-de-Mera, Y., and Rodríguez, D.: Atmospheric sink

715 of styrene, A-methylstyrene, trans-B-methylstyrene and indene: Rate constants and mechanisms of Cl
716 atom-initiated   degradation,   Atmos.   Environ.,   200,   78–89,
717 https://doi.org/10.1016/j.atmosenv.2018.11.059, 2019a.

718 Tajuelo, M., Rodríguez, D., Baeza-Romero, M. T., Díaz-de-Mera, Y., Aranda, A., and Rodríguez, A.:
719 Secondary organic aerosol formation from styrene photolysis and photooxidation with hydroxyl
720 radicals, Chemosphere, 231, 276–286, https://doi.org/10.1016/j.chemosphere.2019.05.136, 2019b.

721 Takeuchi, M. and Ng, N. L.: Chemical composition and hydrolysis of organic nitrate aerosol formed from
722 hydroxyl and nitrate rlanadical oxidation of α-pinene and β-pinene, Atmos. Chem. Phys., 19, 12749–
723 12766, https://doi.org/10.5194/acp-19-12749-2019, 2019.

724 Takeuchi, M., Berkemeier, T., Eris, G., and Ng, N. L.: Non-linear effects of secondary organic aerosol
725 formation and properties in multi-precursor systems, Nat. Commun., 13, 1–13,
726 https://doi.org/10.1038/s41467-022-35546-1, 2022.

727 Takeuchi, M., Wang, Y., Nault, B. A., Chen, Y., Canagaratna, M. R., and Ng, N. L.: Evaluating the response
728 of the Aerodyne aerosol mass spectrometer to monoterpene- and isoprene-derived organic nitrate
729 standards, Aerosol Sci. Technol., 0, 1–18, https://doi.org/10.1080/02786826.2024.2389183, 2024.

730 Tasoglou, A. and Pandis, S. N.: Formation and chemical aging of secondary organic aerosol during the β-
731 caryophyllene oxidation, Atmos. Chem. Phys., 15, 6035–6046, https://doi.org/10.5194/acp-15-6035-
732 2015, 2015.

733 Thornton, J. A., Mohr, C., Schobesberger, S., D'Ambro, E. L., Lee, B. H., and Lopez-Hilfiker, F. D.:
734 Evaluating Organic Aerosol Sources and Evolution with a Combined Molecular Composition and
735 Volatility Framework Using the Filter Inlet for Gases and Aerosols (FIGAERO), Acc. Chem. Res., 53,
736 1415–1426, https://doi.org/10.1021/acs.accounts.0c00259, 2020.

737 Tuazon, E. C., Arey, J., Atkinson, R., and Aschmann, S. M.: Gas-Phase Reactions of 2-Vinylpyridine and
738 Styrene with OH and NO3 Radicals and O3, Environ. Sci. Technol., 27, 1832–1841,
739 https://doi.org/10.1021/es00046a011, 1993.

740 Vasquez, K. T., Crounse, J. D., Schulze, B. C., Bates, K. H., Teng, A. P., Xu, L., Allen, H. M., and
741 Wennberg, P. O.: Rapid hydrolysis of tertiary isoprene nitrate efficiently removes NOx from the
742 atmosphere, Proc. Natl. Acad. Sci. U. S. A., 117, 33011–33016,
743 https://doi.org/10.1073/PNAS.2017442117, 2021.

744 Vidović, K., Lašič Jurković, D., Šala, M., Kroflič, A., and Grgić, I.: Nighttime Aqueous-Phase Formation
745 of Nitrocatechols in the Atmospheric Condensed Phase, Environ. Sci. Technol., 52, 9722–9730,
746 https://doi.org/10.1021/acs.est.8b01161, 2018.

747 Vione, D., Maurino, V., Minero, C., and Pelizzetti, E.: Phenol photonitration upon UV irradiation of nitrite
748 in aqueous solution I: Effects of oxygen and 2-propanol, Chemosphere, 45, 893–902,

749   https://doi.org/10.1016/S0045-6535(01)00035-2, 2001.

750   Vione, D., Maurino, V., Minero, C., Lucchiari, M., and Pelizzetti, E.: Nitration and hydroxylation of

751   benzene in the presence of nitrite/nitrous acid in aqueous solution, Chemosphere, 56, 1049–1059,

752   https://doi.org/10.1016/j.chemosphere.2004.05.027, 2004.

753   Wang, H., Ji, Y., Gao, Y., Li, G., and An, T.: Theoretical model on the formation possibility of secondary

754   organic aerosol from OH initialed oxidation reaction of styrene in the presence of O2/NO, Atmos.

755   Environ., 101, 1–9, https://doi.org/10.1016/j.atmosenv.2014.10.042, 2015.

756   Wang, W., Zhang, Y., Jiang, B., Chen, Y., Song, Y., Tang, Y., Dong, C., and Cai, Z.: Molecular

757   characterization of organic aerosols in Taiyuan, China: Seasonal variation and source identification,

758   Sci. Total Environ., 800, 149419, https://doi.org/10.1016/j.scitotenv.2021.149419, 2021a.

759   Wang, X., Hayeck, N., Brüggemann, M., Yao, L., Chen, H., Zhang, C., Emmelin, C., Chen, J., George, C.,

760   and Wang, L.: Chemical Characteristics of Organic Aerosols in Shanghai: A Study by Ultrahigh-

761   Performance Liquid Chromatography Coupled With Orbitrap Mass Spectrometry, J. Geophys. Res.

762   Atmos., 122, 11,703-11,722, https://doi.org/10.1002/2017JD026930, 2017.

763   Wang, Y., Hu, M., Wang, Y., Zheng, J., Shang, D., Yang, Y., Liu, Y., Li, X., Tang, R., Zhu, W., Du, Z.,

764   Wu, Y., Guo, S., Wu, Z., Lou, S., Hallquist, M., and Yu, J. Z.: The formation of nitro-aromatic

765   compounds under high NOx and anthropogenic VOC conditions in urban Beijing, China, Atmos.

766   Chem. Phys., 19, 7649–7665, https://doi.org/10.5194/acp-19-7649-2019, 2019.

767   Wang, Y., Piletic, I. R., Takeuchi, M., Xu, T., France, S., and Ng, N. L.: Synthesis and Hydrolysis of

768   Atmospherically Relevant Monoterpene-Derived Organic Nitrates, Environ. Sci. Technol., 55, 14595–

769   14606, https://doi.org/10.1021/acs.est.1c05310, 2021b.

770   Wu, S., Tang, G., Wang, Y., Yang, Y., Yao, D., Zhao, W., Gao, W., Sun, J., and Wang, Y.: Vertically

771   decreased VOC concentration and reactivity in the planetary boundary layer in winter over the North

772   China Plain, Atmos. Res., 240, 104930, https://doi.org/10.1016/j.atmosres.2020.104930, 2020.

773   Yang, L. H., Takeuchi, M., Chen, Y., and Ng, N. L.: Characterization of thermal decomposition of

774   oxygenated organic compounds in FIGAERO-CIMS, Aerosol Sci. Technol., 55, 1321–1342,

775   https://doi.org/10.1080/02786826.2021.1945529, 2021.

776   Yang, X., Luo, F., Li, J., Chen, D., Ye, E., Lin, W., and Jin, J.: Alkyl and aromatic nitrates in atmospheric

777   particles determined by gas chromatography tandem mass spectrometry, J. Am. Soc. Mass Spectrom.,

778   30, 2762–2770, https://doi.org/10.1007/s13361-019-02347-8, 2019.

779   Yang, Y., Wang, Y., Zhou, P., Yao, D., Ji, D., Sun, J., Wang, Y., Zhao, S., Huang, W., Yang, S., Chen, D.,

780   Gao, W., Liu, Z., Hu, B., Zhang, R., Zeng, L., Ge, M., Petäjä, T., Kerminen, V. M., Kulmala, M., and

781   Wang, Y.: Atmospheric reactivity and oxidation capacity during summer at a suburban site between

782   Beijing and Tianjin, Atmos. Chem. Phys., 20, 8181–8200, https://doi.org/10.5194/acp-20-8181-2020,

783   2020.

784   Yassine, M. M., Harir, M., Dabek-Zlotorzynska, E., and Schmitt-Kopplin, P.: Structural characterization
785   of organic aerosol using Fourier transform ion cyclotron resonance mass spectrometry: aromaticity
786   equivalent   approach,   Rapid   Commun.   Mass   Spectrom.,   28,   2445–2454,
787   https://doi.org/10.1002/rcm.7038, 2014.

788   Ye, C., Yuan, B., Lin, Y., Wang, Z., Hu, W., Li, T., Chen, W., Wu, C., Wang, C., Huang, S., Qi, J., Wang,
789   B., Wang, C., Song, W., Wang, X., Zheng, E., Krechmer, J. E., Ye, P., Zhang, Z., Wang, X., Worsnop,
790   D. R., and Shao, M.: Chemical characterization of oxygenated organic compounds in the gas phase
791   and particle phase using iodide CIMS with FIGAERO in urban air, Atmos. Chem. Phys., 21, 8455–
792   8478, https://doi.org/10.5194/acp-21-8455-2021, 2021.

793   Yeh, G. K. and Ziemann, P. J.: Gas-wall partitioning of oxygenated organic compounds: Measurements,
794   structure-activity relationships, and correlation with gas chromatographic retention factor, Aerosol Sci.
795   Technol., 49, 727–738, https://doi.org/10.1080/02786826.2015.1068427, 2015.

796   Ylisirniö, A., Barreira, L. M. F., Pullinen, I., Buchholz, A., Jayne, J., Krechmer, J. E., Worsnop, D. R.,
797   Virtanen, A., and Schobesberger, S.: On the calibration of FIGAERO-ToF-CIMS: Importance and
798   impact of calibrant delivery for the particle-phase calibration, Atmos. Meas. Tech., 14, 355–367,
799   https://doi.org/10.5194/amt-14-355-2021, 2021.

800   Yu, K., Zhu, Q., Du, K., and Huang, X.: Characterization of nighttime formation of particulate organic
801   nitrates based on high-resolution aerosol mass spectrometry in an urban atmosphere in China, Atmos.
802   Chem. Phys., 19, 5235–5249, 2019.

803   Yu, L., Smith, J., Laskin, A., Anastasio, C., Laskin, J., and Zhang, Q.: Chemical characterization of SOA
804   formed from aqueous-phase reactions of phenols with the triplet excited state of carbonyl and hydroxyl
805   radical, Atmos. Chem. Phys., 14, 13801–13816, https://doi.org/10.5194/acp-14-13801-2014, 2014.

806   Yu, L., Smith, J., Laskin, A., M George, K., Anastasio, C., Laskin, J., M Dillner, A., and Zhang, Q.:
807   Molecular transformations of phenolic SOA during photochemical aging in the aqueous phase:
808   Competition among oligomerization, functionalization, and fragmentation, Atmos. Chem. Phys., 16,
809   4511–4527, https://doi.org/10.5194/acp-16-4511-2016, 2016.

810   Yu, S., Jia, L., Xu, Y., and Pan, Y.: Formation of extremely low-volatility organic compounds from styrene
811   ozonolysis: Implication   for   nucleation,   Chemosphere,   305,   135459,
812   https://doi.org/10.1016/j.chemosphere.2022.135459, 2022a.

813   Yu, S. S., Jia, L., Xu, Y. F., and Pan, Y. P.: Molecular composition of secondary organic aerosol from
814   styrene   under   different   NOx   and   humidity   conditions,   Atmos.   Res.,   266,   105950,
815   https://doi.org/10.1016/j.atmosres.2021.105950, 2022b.

816   Zare, A., Fahey, K. M., Sarwar, G., Cohen, R. C., and Pye, H. O. T.: Vapor-Pressure Pathways Initiate but

817   Hydrolysis Products Dominate the Aerosol Estimated from Organic Nitrates, ACS Earth Sp. Chem.,

818   3, 1426–1437, https://doi.org/10.1021/acsearthspacechem.9b00067, 2019.

819 Zhang, X., Cappa, C. D., Jathar, S. H., McVay, R. C., Ensberg, J. J., Kleeman, M. J., and Seinfeld, J. H.:

820   Influence of vapor wall loss in laboratory chambers on yields of secondary organic aerosol, Proc. Natl.

821   Acad. Sci. U. S. A., 111, 5802–5807, https://doi.org/10.1073/pnas.1404727111, 2014.

822 Zhang, X., Schwantes, R. H., McVay, R. C., Lignell, H., Coggon, M. M., Flagan, R. C., and Seinfeld, J. H.:

823   Vapor wall deposition in Teflon chambers, Atmos. Chem. Phys., 15, 4197–4214,

824   https://doi.org/10.5194/acp-15-4197-2015, 2015.

825 Zhang, Y., Pei, C., Zhang, J., Cheng, C., Lian, X., Chen, M., Huang, B., Fu, Z., Zhou, Z., and Li, M.:

826   Detection of polycyclic aromatic hydrocarbons using a high performance-single particle aerosol mass

827   spectrometer, J. Environ. Sci. (China), 124, 806–822, https://doi.org/10.1016/j.jes.2022.02.003, 2023.

828 Zhang, Z., Wang, H., Chen, D., Li, Q., Thai, P., Gong, D., Li, Y., Zhang, C., Gu, Y., Zhou, L., Morawska,

829   L., and Wang, B.: Emission characteristics of volatile organic compounds and their secondary organic

830   aerosol formation potentials from a petroleum refinery in Pearl River Delta, China, Sci. Total Environ.,

831   584–585, 1162–1174, https://doi.org/10.1016/j.scitotenv.2017.01.179, 2017.

832

833   **Table 1**. Summary of experimental conditions in this study.

Exp	RH	Seed	ΔHC (ppb)[b]	ΔHC (μg m^{-3})	N_2O_5 (ppb)	HC:N_2O_5 Ratio	ΔM$_O$ (μg m^{-3})[c,d]	SOA Mass yield (%)
1	<3%	AS[a]	9.5 ± 0.3	40.7 ± 1.3	20	1:2	1.9 ± 0.2	4.5 ± 0.5
2	<3%	AS	15.6 ± 0.2	67.1 ± 0.8	36	1:2	5.4 ± 0.2	8.1 ± 0.4
3	<3%	AS	18.0 ± 0.1	77.6 ± 0.5	40	1:2	6.8 ± 0.3	8.6 ± 0.4
4	<3%	AS	28.4 ± 0.5	122.0 ± 2.0	60	1:2	12.4 ± 0.6	10.1 ± 0.5
5	<3%	AS	48.2 ± 1.0	207.2 ± 4.2	100	1:2	26.1 ± 0.4	12.6 ± 0.2
6	<3%	AS	80.1 ± 0.7	344.4 ± 3.1	160	1:2	48.5 ± 0.7	14.1 ± 0.2
7	<3%	AS	99.1 ± 0.8	426.0 ± 3.4	200	1:2	67.0 ± 1.0	15.7 ± 0.2
8	<3%	AS	155.2 ± 1.8	667.5 ± 7.9	310	1:2	107.4 ± 0.5	16.1 ± 0.1
9	<3%	None	18.2 ± 0.5	78.3 ± 2.2	40	1:2	0.6 ± 0.1	0.81 ± 0.1
10	<3%	None	100.4 ± 0.8	431.8 ± 3.5	200	1:2	47.6 ± 0.8	11.03 ± 0.2
11	50%	AS	17.3 ± 0.2	74.5 ± 0.8	40	1:2	/[e]	/[e]
12	70%	AS	15.8 ± 0.5	67.8 ± 1.9	40	1:2	/[e]	/[e]

[a.] Ammonium sulfate. [b.] Uncertainties in hydrocarbon concentration are calculated from 1 standard deviation from GC-FID measurements. [c.] Uncertainties in aerosol mass loading are calculated from 1 standard deviation of aerosol volume as measured by the SMPS. [d.] Density is 1.35 g m^{-3}, calculated from the comparison of HR-ToF-AMS and SMPS size distribution data. [e.] These numbers are not reported because the density of SOA in humid experiments is not available.
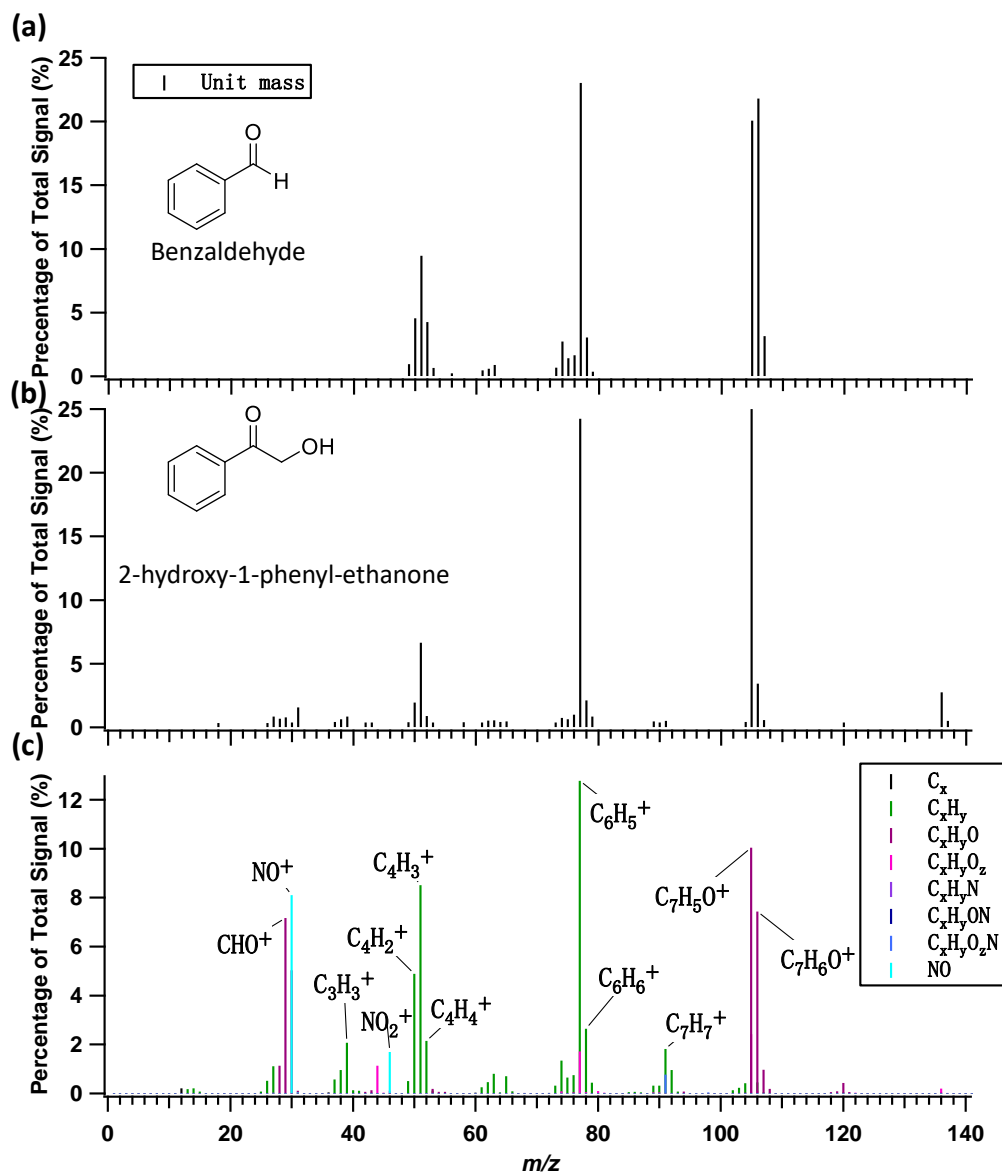
834
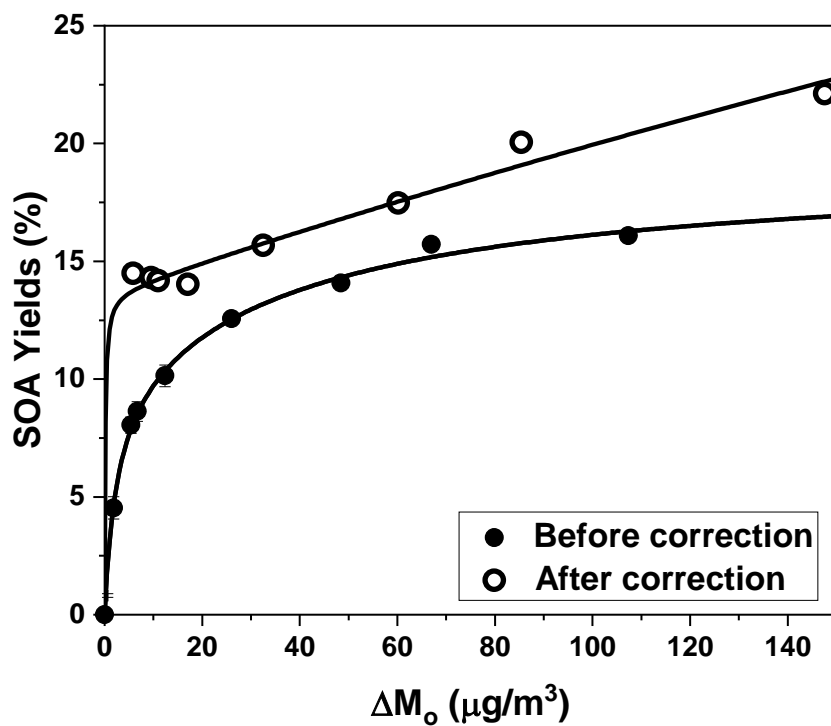
Figure 1. SOA yield data and yield curves for styrene+NO$_3$ oxidation with and without vapor wall loss correction.
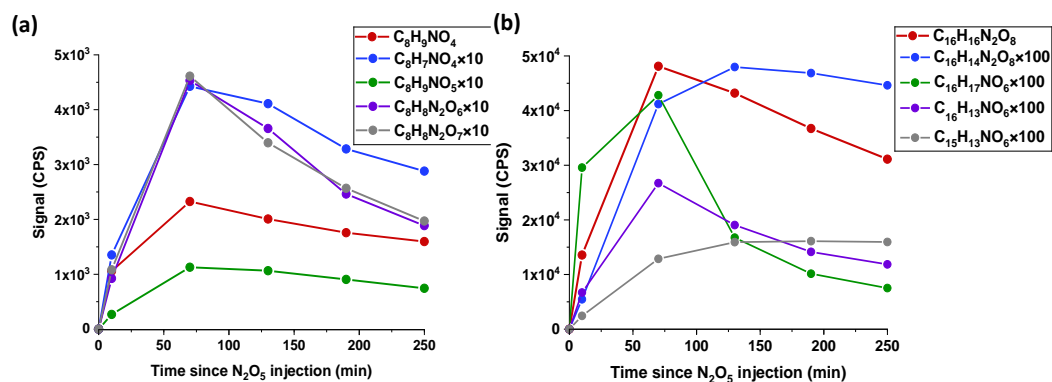
838

839

840
Figure 2. Comparison between the National Institute of Standards and Technology (NIST) mass spectra of
(a) benzaldehyde; (b) 2-hydroxy-1-phenyl ethenone; and (c) the HR-ToF-AMS mass spectrum (in integer
m/z) of SOA from styrene+NO_3 oxidation. The chemical structures for benzaldehyde and 2-hydroxy-1-
phenyl ethenone are shown in (a) and (b).

Figure 3. (a) A typical FIGAERO-CIMS mass spectrum of SOA from styrene+NO_3 oxidation (Exp. 7). The sticks are colored to distinguish between monomeric and dimeric products, as indicated in the legend. Prominent masses are labeled with the corresponding chemical formulae without an iodide ion. Only *m/z* 250-500 are shown here, there are no specific major products before *m/z* 250 except I^- and HNO_3I^- ; (b) SOA product distribution, categorized by molecule types: CHO, CHON, and $CHON_2$. Each category is further subdivided by carbon number; (c) The pie chart illustrates the relative percentage contributions of CHO, CHON, and $CHON_2$.

Figure 4. The time series of major particle-phase products from styrene+NO_3 oxidation measured by FIGAERO-CIMS, including: (a) monomeric styrene ONs; and (b) dimeric styrene ONs.
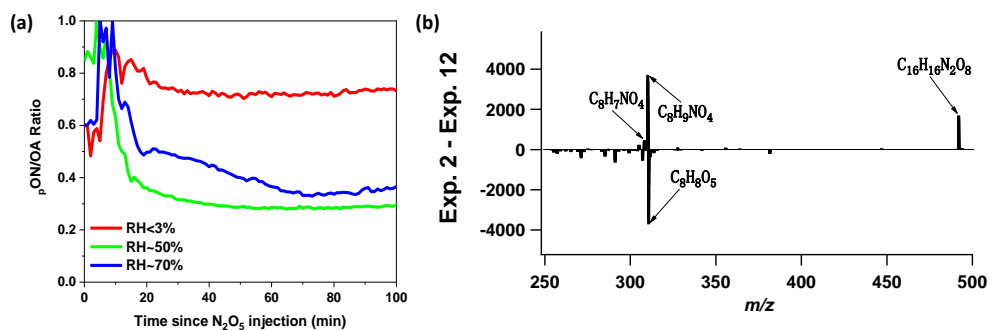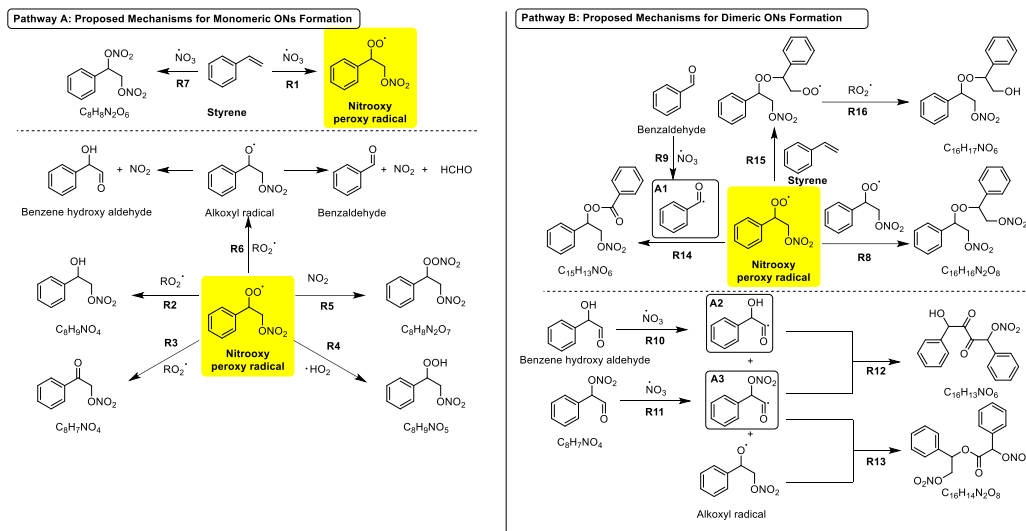
Figure 5. (a) Time series data of the ratio of particulate ONs ($_p$ON) to total organic aerosols (OA) in Exp. 2 (RH<3%), Exp. 11 (RH~50%), and Exp. 12 (RH~70%); (b) FIGAERO-CIMS difference mass spectrum of SOA: Exp. 2 (RH<3%) minus Exp. 12 (RH~70%). Prominent masses are labeled with the corresponding chemical formulae without an iodide ion.

862

863
864 **Figure 6.** The proposed formation mechanisms for the major particle-phase products resulting from

865 styrene+NO$_3$ oxidation includes two distinct pathways: Pathway A is the proposed formation pathway for

866 monomeric ON products. Pathway B is the proposed formation pathway for dimeric ON products. Radicals

867 A1, A2, and A3 are highlighted in the boxes as the major products resulting from the reaction between

868 aldehydes and NO$_3$ radicals. The nitrooxy peroxy radical is highlighted in yellow as the major RO$_2$ in

869 mechanisms.